

Least action description of spontaneous fission in fermium and nobelium nuclei based on the Gogny energy density functional

R. Rodríguez-Guzmán¹ and L. M. Robledo^{2,3}

¹*Physics Department, Kuwait University, 13060 Kuwait, Kuwait*

²*Center for Computational Simulation, Universidad Politécnica de Madrid, Campus de Montegancedo, Boadilla del Monte, 28660-Madrid. Spain*

³*Departamento de Física Teórica, Universidad Autónoma de Madrid, E-28049 Madrid, Spain*

(Dated: June 23, 2021)

The systematic of the spontaneous fission half-lives for the nuclei $^{242-262}\text{Fm}$ and $^{250-260}\text{No}$ is analyzed, within a least action scheme, with the parametrization DIM of the Gogny energy density functional. The properties of the dynamic (least action) fission paths are analyzed and compared to those of the static (minimal energy) ones. The constrained Hartree-Fock-Bogoliubov approximation is used to compute deformed mean-field configurations, zero-point quantum corrections and collective inertias. It is shown that a cumbersome full variational search of the least action fission path, within the space of HFB states, might not be required if the relevant degrees of freedom are taken into account in the minimization of the Wentzel-Kramers-Brillouin action. The action is minimized in terms of pairing fluctuations that explore the pairing content of the HFB states along the fission paths of the considered nuclei. It is found that, for a given shape, the minimum of the action in fermium and nobelium nuclei corresponds to a value of the pairing fluctuations larger than the one associated with the minimal energy solution for the same shape. The reduction of the action, via larger pairing correlations, has a significant impact on the predicted spontaneous fission half-lives improving their comparison with the experiment by several orders of magnitude.

PACS numbers: 24.75.+i, 25.85.Ca, 21.60.Jz, 27.90.+b, 21.10.Pc

I. INTRODUCTION

Disentangling which are the most relevant degrees of freedom in the fission of the atomic nucleus still remains a major challenge in today's nuclear structure physics [1–4]. Fission is traditionally portrayed as the smooth evolution of the nuclear shape from the one of the ground state to the shape at scission. Shape evolution is governed by both subtle quantum mechanics effects and the competition of global properties of the nuclear interaction like surface properties and Coulomb repulsion. The dynamics of shape evolution is usually described in terms of a Hartree-Fock-Bogoliubov (HFB) mean field with constrains on some deformation parameters \mathbf{Q} like the quadrupole moment, hexadecapole moment or necking. The evolution of the energy with deformation leads to a potential energy curve (or surface, in the general case) (PES) that, along with some collective inertias, can be used to determine fission observables like spontaneous fission lifetimes (t_{SF}) which are traditionally computed within the Wentzel-Kramers-Brillouin (WKB) framework used to describe tunneling through a barrier. Super-heavy nuclei ($Z > 100$) belong to the class of nuclei where there is no classical fission barrier and therefore only quantal effects are responsible for their stability. Therefore, they are the perfect laboratory to understand the subtle quantal effects relevant in the dynamics of fission [5]. The insight gained on the properties of those quantal effects can provide key information on the very limits of nuclear stability and the existence of super-heavy nuclei beyond Oganesson [6]. Among super-heavy nuclei, extensive experimental studies [7] have been able

to determine the spontaneous fission lifetime of a wealth of isotopes of fermium and nobelium. On the other hand, the reproduction of the inverted parabola behavior of t_{SF} as a function of neutron number characteristic of both isotopic chains has been a challenge for microscopic mean field models. For these reasons, we have chosen the two mentioned isotopic chains as the subject of our present study.

In recent years, the constrained mean-field approximation [8] has emerged as a useful tool to study the gross features of fission from a microscopic perspective [4]. Calculations are typically carried out with (effective) non-relativistic interactions like Gogny [9–17], Skyrme [18–22], and Barcelona-Catania-Paris-Madrid (BCPM) [23–25] or with relativistic [26–30] energy density functionals (EDFs). One of the main outcomes of those mean-field calculations is the potential energy surface given as a function of quadrupole, octupole, . . . , or necking deformation parameters $\mathbf{Q} = (Q_{20}, Q_{22}, Q_{30}, \dots, Q_{Neck})$ and determined by self-consistent HFB constrained calculations. Moreover, the mean-field framework also provides the associated collective inertias as well as the quantum zero-point rotational and vibrational energy corrections. All those ingredients are required to compute fission observables like, for example, the spontaneous fission half-lives t_{SF} . Some studies [5, 30–32] comparing the predictions of the different interactions just mentioned come to the conclusion that the differences found among them are at the quantitative, not the qualitative, level.

Within the standard approach, the HFB wave functions along the fission path are obtained by minimizing the constrained HFB energy in accordance to the Ritz

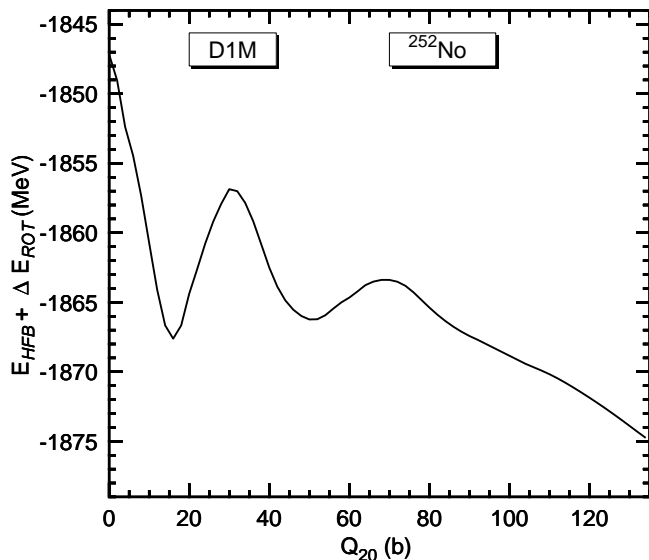


FIG. 1: The HFB plus rotational correction energy corresponding to the static fission path is plotted, as a function of the quadrupole moment Q_{20} , for the nucleus ^{252}No .

variational principle [8]. In the last few years we have resorted to this approach to describe the fission properties of even-even Ra, U and Pu nuclei as well as for a selected set of super-heavy elements [33–35] using the three most important parametrizations of the Gogny-EDF, namely, D1M [36], D1N [37] and D1S [9]. Special attention has also been paid to understand the uncertainties in the predicted t_{SF} values arising from the different building blocks entering the semi-classical WKB formula used to compute them. For instance, it has been found in those studies that modifications of a few per cent in the pairing strengths can have a significant impact on the collective masses leading to uncertainties of several orders of magnitude in the predicted t_{SF} values. Though there is a large variability of the predicted t_{SF} values with respect to the details involved in their computation, it has also been shown that this mean field framework produces a robust trend with neutron number for the considered even-even nuclei and the changes in the different building blocks only amount to a parallel displacement of the curves. Similar conclusions can be extracted from recent fission studies for odd-mass U, Pu and No nuclei [40, 41] within the Equal Filling Approximation (EFA) [42].

The calculations mentioned above belong to the so called "static" category where the guiding principle is the least energy principle. This is considered to be just an approximation to the "least action" principle, known as the "dynamic" approach, involving the minimization of the action associated with a given set of relevant coordinates. It is thought that the dynamic approach is better suited to describe the tunneling through the barrier. It is well known that both the static and dynamic approaches provide similar results [43, 44] when considering only shape degrees of freedom. This is the traditional

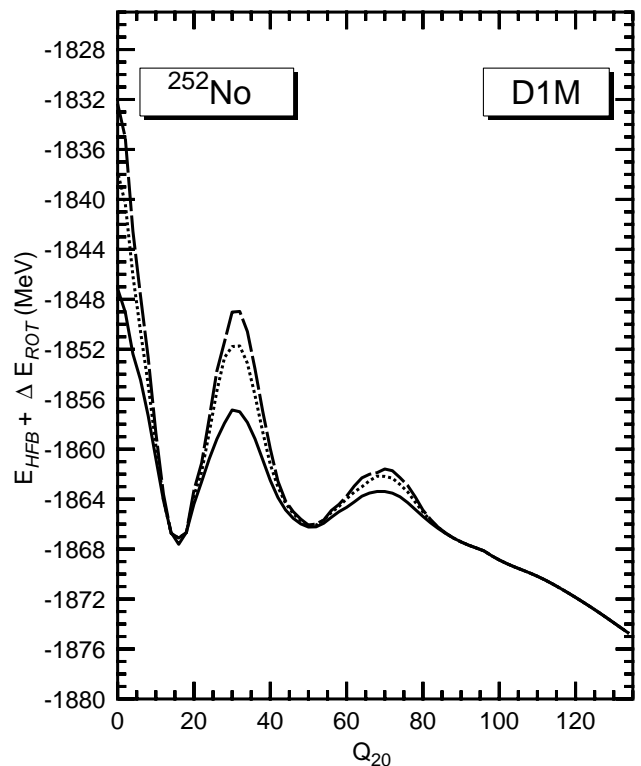


FIG. 2: The HFB plus rotational correction energy corresponding to the dynamic ATDHFB (dashed line) and GCM (dotted line) fission paths are plotted, as functions of the quadrupole moment Q_{20} , for the nucleus ^{252}No . The energies corresponding to the static path (full line) are also included in the plot. For details, see the main text.

justification for using the simpler static approach. However, the key role played by pairing degrees of freedom in the dynamics of fission was already pointed out in Ref. [45]. It was found that the competition between the collective inertia (decreasing as the inverse of the square of the pairing gap [46, 47]) and the energy (increasing as the square of the pairing gap) leads to a minimum of the action at a larger pairing gap than the one corresponding to the minimum energy approach. A number of spontaneous fission studies have already considered the effect of pairing fluctuations in fission [48–54] showing that including pairing as a dynamical variable produces a reduction of a few orders of magnitude in the computed t_{SF} values as compared to the ones obtained within the static approach. Moreover, pairing fluctuations can also restore axial symmetry along the fission path [52, 53].

Another observable of interest is the fission fragments' mass distribution. This quantity can be studied microscopically within time dependent approximations like the Time Dependent Generator Coordinate Method (TDGCM) [55–59], stochastic time dependent HF+BCS [60] or the Time Dependent HFB (TDHFB) [61–63] requiring enormous computational resources. It has been shown [58] that increasing the pairing strength by a few percent modifies in a substantial way the fragments' mass

distribution, showing the relevance of the pairing degree of freedom also in this respect. Therefore, it would be very interesting to extend the present framework, based on the least action principle, to the time dependent case, but this is out of the scope of this paper.

Recently, we have studied the predictions for spontaneous fission half-lives within a least action scheme based on the Gogny-D1M EDF for a selected set of U isotopes [44]. On the one hand, our calculations corroborate that the static and dynamic approaches lead to similar results when shape degrees of freedom are the only ones considered. On the other hand, the results show the large impact on the action coming from the particle number fluctuation ($\langle \Delta \hat{N}^2 \rangle$) degree of freedom (a quantity connected with pairing correlations). For a given nuclear shape, labeled by the quadrupole moment Q_{20} , the minimum of the action, in the direction of the $\langle \Delta \hat{N}^2 \rangle$ variable, can be up to a factor of three smaller than the value of the action for the minimum energy state with the same Q_{20} value. This reduction has a strong impact on the predicted t_{SF} values and dramatically improves the agreement with the experiment in the case of $^{232-238}\text{U}$.

In this paper we consider again the particle number fluctuation ($\langle \Delta \hat{N}^2 \rangle$) as the relevant degree of freedom in the minimization of the action and use this framework to compute the spontaneous fission half-lives for the super-heavy isotopes $^{242-262}\text{Fm}$ and $^{250-260}\text{No}$. The choice is driven by the existence of experimental data for those isotopes [7] and also because they belong to a region of the nuclear chart where the shell effects characteristic of super-heavy elements with $Z > 100$ start to manifest [17, 40]. Moreover, accounting for the experimental bell-shaped dependence of the spontaneous fission half-lives as functions of the neutron number [7] in fermium and nobelium nuclei represents a very challenging test for any model of fission.

In the calculations we have used the Gogny-D1M EDF [36]. The suitability of the Gogny-D1M EDF to describe fission in heavy and super-heavy nuclei has been demonstrated in previous studies [33–35, 40, 41] where the results for barrier heights, excitation energies of fission isomers and half-lives have shown a good agreement with experimental data. The comparison with other theoretical studies using other parametrizations [10, 15, 17, 24] is also satisfactory. This is a nice feature as the parametrization D1M does a much better job in reproducing nuclear masses [36] than D1S. In addition, D1M performs as well as D1S in the description of nuclear structure phenomena [64–70].

The paper is organized as follows. In Sec. II, we briefly outline the procedure to find the least action path using the quadrupole moment Q_{20} and particle number fluctuation ($\langle \Delta \hat{N}^2 \rangle$) as relevant coordinates. The results of our calculations are discussed in Sec. III. First, in Sec. III A, we illustrate the method in the case of ^{252}No . The systematic of the spontaneous fission half-lives in $^{242-262}\text{Fm}$ and $^{250-260}\text{No}$ and the properties of the least action paths are presented in Sec. III B where we also compare with

results obtained within the static framework. Finally, Sec. IV is devoted to the concluding remarks and work perspectives.

II. THEORETICAL FRAMEWORK

The mean-field approximation based on (product) HFB wave functions [8] has been used in the present study. Constrains in the mean value of the axially symmetric quadrupole \hat{Q}_{20} and octupole \hat{Q}_{30} operators as well as on the particle number fluctuations $\Delta \hat{N}^2$ [44] have been used. Though it will not be mentioned explicitly, in all the HFB calculations discussed below, aside from the usual constrains on both the proton and neutron numbers [8], a constrain on the operator \hat{Q}_{10} is used to prevent spurious effects associated to the center of mass motion. Note, that parity is allowed to be broken at any stage of the calculations as required by the physics of asymmetric fission.

The HFB quasiparticle operators, have been expanded in an axially symmetric (deformed) harmonic oscillator (HO) basis containing states with J_z quantum numbers up to $35/2$ and up to 26 quanta in the z direction. They correspond to those satisfying the condition $2n_{\perp} + |m| + qn_z \leq M_{z,\text{MAX}}$ with $M_{z,\text{MAX}} = 17$ and $q = 1.5$. This choice is well suited for the elongated prolate shapes typical of the fission process [15, 24]. The two HO lengths b_z and b_{\perp} have been optimized so as to minimize the total HFB energy for each value of the quadrupole moment. The computationally expensive oscillator length optimization along with the large HO basis used guarantees good convergence in the potential energy surface in the relevant range of shape deformation [15]. An approximate second order gradient method [71] has been used for the solution of the HFB equation. The main reason for this choice is the clear advantage of this type of methods over the more traditional successive diagonalization method when many constrains are imposed. As it is customary in all the Gogny force parametrizations, the two-body kinetic energy correction, including the exchange and pairing channels, has been taken into account in the Ritz-variational procedure. On the other hand, the Coulomb exchange term is considered in the Slater approximation [72] while the Coulomb and spin-orbit contributions to the pairing field have been neglected.

Within the WKB formalism the t_{SF} half-life (in seconds) is given by

$$t_{SF} = 2.86 \times 10^{-21} \times (1 + e^{2S}) \quad (1)$$

where the action S along the (one-dimensional Q_{20} -projected) fission path reads

$$S = \int_a^b dQ_{20} \mathcal{S}(Q_{20}) \quad (2)$$

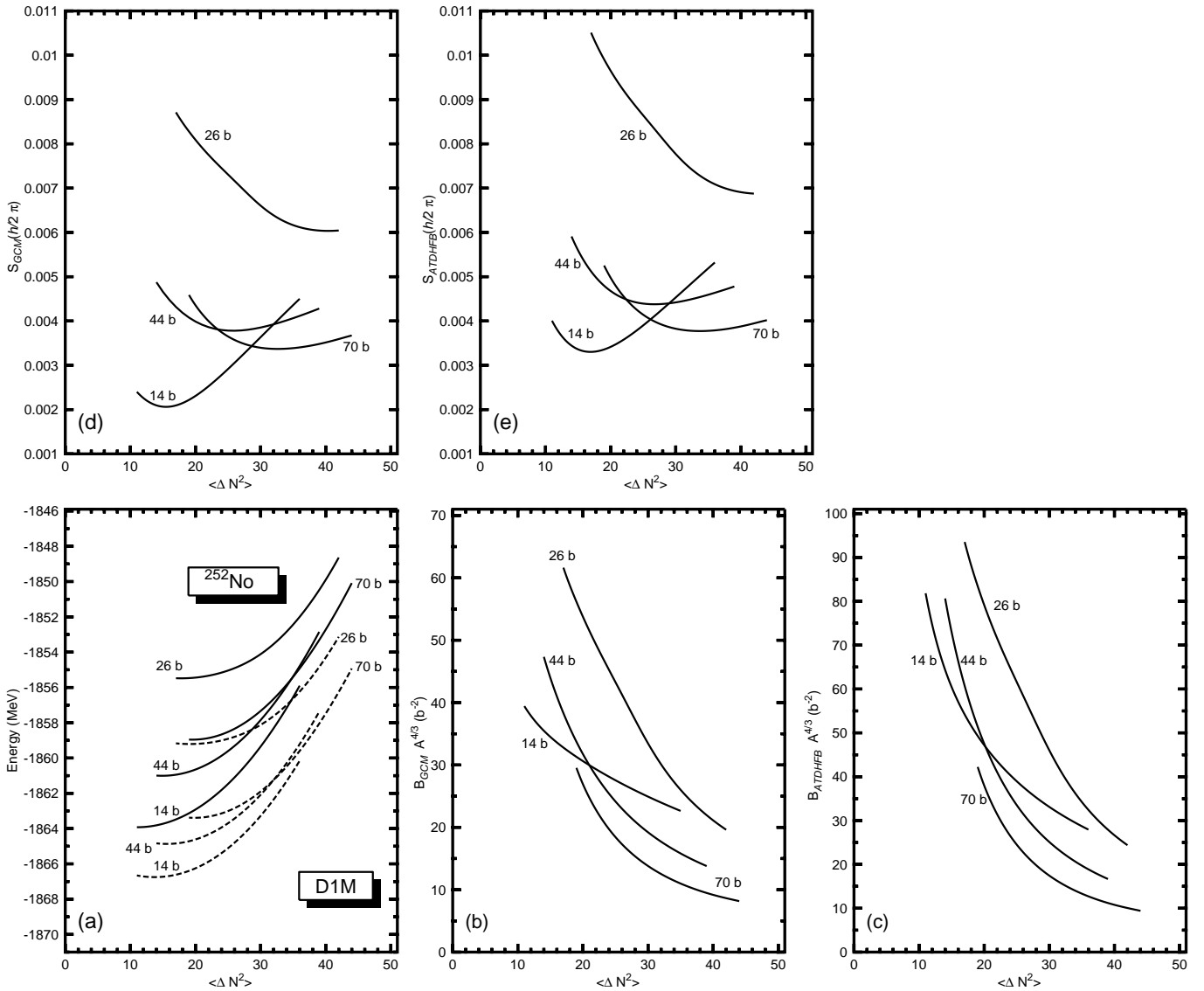


FIG. 3: The intrinsic HFB energies (full lines) and the HFB plus rotational correction energies (dashed lines) [panel (a)], GCM and ATDHFB collective masses [panels (b) and (c)] as well as the GCM and ATDHFB integrand of the action Eq.(2) [panels (d) and (e)], are plotted as functions of the particle number fluctuations $\langle \Delta \hat{N}^2 \rangle$. Results are shown for the quadrupole moments $Q_{20} = 14, 26, 44$ and 70 b. For more details, see the main text.

and the integrand $\mathcal{S}(Q_{20})$ takes the form

$$\mathcal{S}(Q_{20}) = \sqrt{2B(Q_{20}) (V(Q_{20}) - (E_{Min} + E_0))} \quad (3)$$

The integration limits a and b are the classical turning points [46] for the potential $V(Q_{20})$ corresponding to the energy $E_{Min} + E_0$. The energy E_{Min} corresponds to the ground state minimum for the considered path while E_0 accounts for the true ground state energy once quadrupole fluctuations are taken into account. In this work, we have taken the typical value $E_0 = 0.5$ MeV [15, 17]. In Eq.(3), $B(Q_{20})$ represents the collective mass. The potential $V(Q_{20})$ is given by the HFB energy corrected by the zero-point vibrational and rotational energies. For the evaluation of the collective mass and

the zero-point vibrational energy correction two methods have been used. One is the cranking approximation [73–75] to the Adiabatic Time Dependent HFB (ATDHFB) scheme. The second method is based on the Gaussian Overlap Approximation (GOA) to the GCM. Details on how to compute the required quantities can be found, for instance, in Refs. [3, 4]. As it is customary in fission calculations, the coupling with other degrees of freedom in the evaluation of the collective mass is neglected within both the ATDHFB and GCM schemes [44] and only the quadrupole inertia is considered. The rotational energy correction ΔE_{ROT} has been computed in terms of the Yoccoz moment of inertia [76–78].

In order to compute t_{SF} using the least action frame-

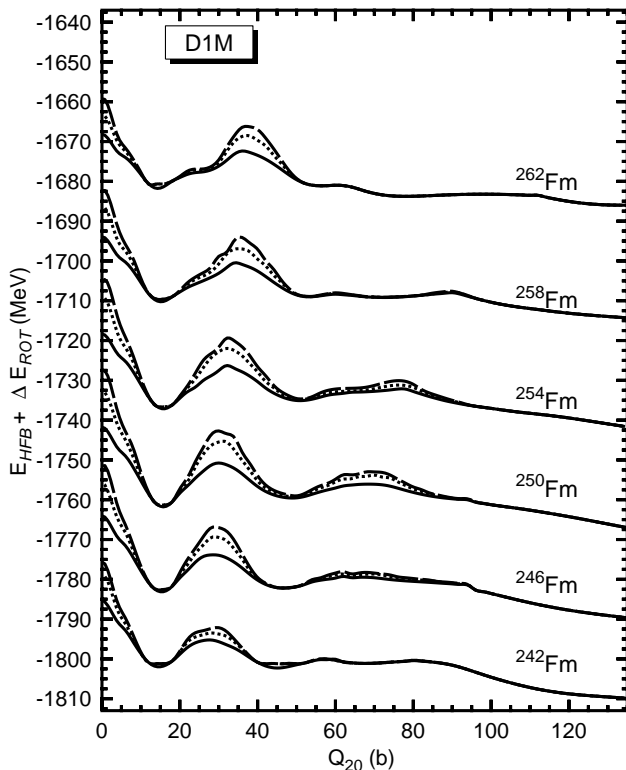


FIG. 4: The HFB plus rotational correction energies corresponding to the dynamic ATDHFB (dashed line) and GCM (dotted line) fission paths are plotted as functions of the quadrupole moment Q_{20} for the nuclei $^{242,246,250,254,258,262}\text{Fm}$. The energies corresponding to the static paths (full line) are also included in the plot. Starting from the nucleus ^{246}Fm , the curves have been shifted by 50 MeV in order to accommodate them in a single plot. For details, see the main text.

work we have followed the procedure described below in order to find a good approximation to the least action path. To illustrate the practical aspects of the methodology employed we use the nucleus ^{252}No as an example.

Step 1: We have first determined the least energy (i.e., static) fission path for ^{252}No as a function of the axially symmetric quadrupole moment Q_{20} using the HFB mean field procedure. Zero-point quantum rotational and vibrational energies have been added *a posteriori* to the HFB energies.

The static fission path obtained for ^{252}No is depicted in Fig. 1 where the HFB plus rotational correction energy, is plotted as a function of the quadrupole moment. The ground state is located at $Q_{20} = 16$ b and is reflection symmetric. The fission isomer at $Q_{20} = 52$ b lies 1.38 MeV above the ground state from which, it is separated by the inner barrier ($Q_{20} = 30$ b) with the height of 10.75 MeV. As in the ground state case, the fission isomer is also reflection symmetric. Octupole correlations play a key role for quadrupole deformations

$Q_{20} \geq 62$ b. Those correlations significantly affect the outer barrier ($Q_{20} = 70$ b) whose height is 4.23 MeV.

It should be kept in mind that the mean values of the hexadecapole \hat{Q}_{40} and higher multipolarity operators are automatically given by the Ritz-variational procedure that determines the HFB states $|\varphi(Q_{20})\rangle$ corresponding to each of the intrinsic configurations along the static fission path shown in Fig. 1. To each of the states $|\varphi(Q_{20})\rangle$ also corresponds a self-consistent value of the particle number fluctuations $\langle\Delta\hat{N}^2\rangle_{self}$.

Step 2: For each of the different Q_{20} -configurations along the static path of ^{252}No obtained in Step 1, we have performed a set of HFB calculations with constrains on both $\Delta\hat{N}^2$ and \hat{Q}_{20} . The constrained value of $\Delta\hat{N}^2$ starts at the self-consistent value $\langle\Delta\hat{N}^2\rangle_{self}$ and is increased until the minimum of the action of Eq. (2) is reached. We use a small step size and typically of the order of 20-30 values of $\langle\Delta\hat{N}^2\rangle$ are considered. In principle one should vary independently the particle number fluctuation for protons and neutrons but this would have a great impact on the computational cost of the calculation. We have also checked that an independent variation of protons and neutrons do not bring much as compared to the variation of the total particle number fluctuation. This minimization search is performed for both the action obtained with the ATDHFB collective inertia as well as the one with the GCM collective mass. In this way we obtain two dynamically determined paths which have energies larger than the ones of the minimum energy path but for which the corresponding actions are minimized. By using this approximate way to find the minimum action configuration we avoid the use of sophisticated linear programming techniques required by the full minimization approach.

III. DISCUSSION OF THE RESULTS

In this section, we discuss the results of our calculations. First, in Sec. III A, we illustrate the methodology employed to compute the dynamic path in the case of ^{252}No . The same methodology is employed for all the studied nuclei. The systematic of the dynamic paths and spontaneous fission half-lives in $^{242-262}\text{Fm}$ and $^{250-260}\text{No}$ is presented in Sec. III B.

A. An illustrative example: the nucleus ^{252}No

The HFB plus rotational correction energies corresponding to the dynamic ATDHFB and GCM fission

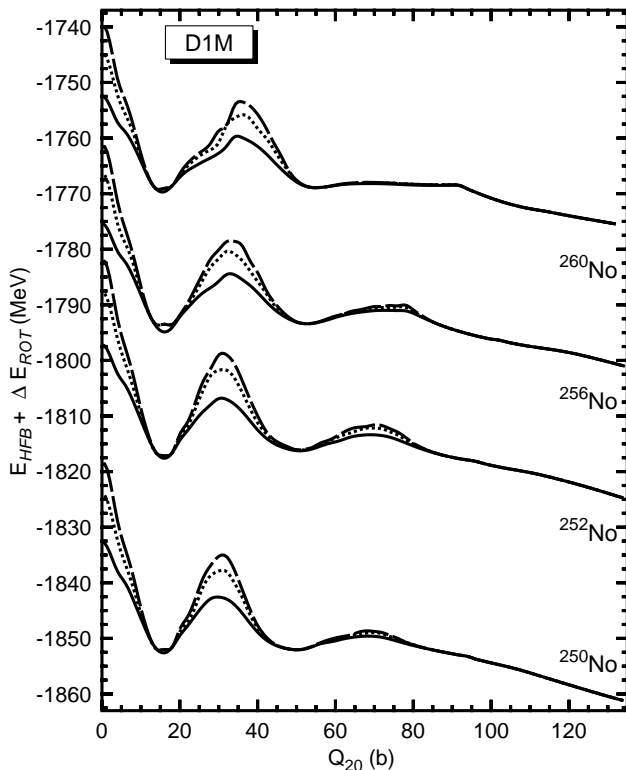


FIG. 5: The HFB plus rotational correction energies corresponding to the dynamic ATDHFB (dashed line) and GCM (dotted line) fission paths are plotted as functions of the quadrupole moment Q_{20} for the nuclei $^{250,252,256,260}\text{No}$. The energies corresponding to the static paths (full line) are also included in the plot. Starting from the nucleus ^{252}No , the curves have been shifted by 50 MeV in order to accommodate them in a single plot. For details, see the main text.

paths are plotted as functions of the quadrupole moment Q_{20} in Fig. 2 for the nucleus ^{252}No . The energies corresponding to the static path are also included in the plot for the sake of comparison.

The deformations of the absolute minimum ($Q_{20} = 16$ b), the top of the inner barrier ($Q_{20} = 30$ b), the fission isomer ($Q_{20} = 52$ b) and the top of the outer barrier ($Q_{20} = 70$ b) corresponding to the dynamic path are similar to those for the static path. In the case of the dynamic path, octupole correlations also play a key role for $Q_{20} \geq 62$ b. However, the dynamic path displays larger inner and outer barrier heights than the static one. The ATDHFB inner (outer) barrier height amounts to 18.09 (5.53) MeV while the GCM inner (outer) barrier height turns out to be 15.38 (4.94) MeV. These numbers should be compared with the values 10.75 and 4.23 MeV for the inner and outer barrier heights of the static path. Large differences are also found at the spherical configuration lying 34.78, 29.31 and 20.46 MeV above the absolute minima of the least action ATDHFB, GCM and the static paths, respectively. Obviously, both kinds of barriers (static and dynamic) can not be compared as they come from different approaches but the big differ-

ences observed raise the question about the suitability of comparing the minimum energy barrier heights with the experimentally determined ones [79].

As mentioned above (see, Sec. II), in order to minimize the action, we have carried out $\Delta\hat{N}^2$ -constrained HFB calculations for each Q_{20} -configuration along the static fission path of ^{252}No . We have started at the self-consistent value $\langle\Delta\hat{N}^2\rangle_{self}$ for each Q_{20} . As an example, in panel (a) of Fig. 3, we have plotted the intrinsic HFB energies (full lines) and the HFB plus the zero-point rotational energies (dashed lines) as functions of the particle number fluctuations $\langle\Delta\hat{N}^2\rangle$ for relevant Q_{20} values, namely 14, 26, 44 and 70 b. For example, for $Q_{20} = 44$ b, $\langle\Delta\hat{N}^2\rangle_{self} = 14$ and we have considered $14 \leq \langle\Delta\hat{N}^2\rangle \leq 39$ with a mesh $\delta\langle\Delta\hat{N}^2\rangle = 1$. As can be seen, the intrinsic HFB energies exhibit an almost parabolic behavior as functions of $\langle\Delta\hat{N}^2\rangle$ with a minimum at $\langle\Delta\hat{N}^2\rangle = \langle\Delta\hat{N}^2\rangle_{self}$. The same is also true for the HFB plus the zero-point rotational energy.

As it is well known, the ATDHFB masses are typically larger than the GCM ones [24, 33–35, 38, 40, 41]. As a consequence, the action in the exponent defining t_{SF} Eq.(1) is, in the ATDHFB case, larger than the GCM one. Depending on the value of the action, this difference can represent a change of several orders of magnitude in the predicted t_{SF} values [33–35, 40, 41]. This is the reason to consider both kinds of collective inertias in this study. In panels (b) and (c) of Fig. 3, we have plotted the GCM and ATDHFB inertias as functions of $\langle\Delta\hat{N}^2\rangle$ for $Q_{20} = 14, 26, 44$ and 70 b. Regardless of the numerical differences between both schemes, the collective masses decrease for increasing $\langle\Delta\hat{N}^2\rangle$. This agrees well with the inverse dependence of the collective masses on the square of the pairing gap [46, 47].

The behavior of $\mathcal{S}(Q_{20})$ Eq.(3) as a function of $\langle\Delta\hat{N}^2\rangle$ for given values of $Q_{20} = 14, 26, 44$ and 70 b is plotted in panels (d) and (e) of Fig. 3. Both the GCM and ATDHFB actions are given. As can be seen, the integrand displays a minimum at a value $\langle\Delta\hat{N}^2\rangle$ substantially larger than the one corresponding to the self-consistent minimal energy solution, i.e., $\langle\Delta\hat{N}^2\rangle_{self}$. For example, in the $Q_{20} = 44$ b case, $\langle\Delta\hat{N}^2\rangle_{self} = 14$ and $\mathcal{S}_{GCM}(Q_{20} = 44b) = 4.8757 \times 10^{-3} \hbar$. As a function of $\langle\Delta\hat{N}^2\rangle$, the minimum value of $\mathcal{S}_{GCM}(Q_{20} = 44b)$ turns out to be $3.7799 \times 10^{-3} \hbar$ and corresponds to $\langle\Delta\hat{N}^2\rangle = 26$. In the ATDHFB case, $\mathcal{S}_{ATDHFB}(Q_{20} = 44b) = 5.9091 \times 10^{-3} \hbar$ for $\langle\Delta\hat{N}^2\rangle_{self} = 14$ while, the minimum value of $\mathcal{S}_{ATDHFB}(Q_{20} = 44b)$ turns out to be $4.3781 \times 10^{-3} \hbar$ for $\langle\Delta\hat{N}^2\rangle = 27$. This kind of quenching, within both the GCM and ATDHFB schemes, reduces considerably the action S Eq.(2) that appears in the exponential of the spontaneous fission half-life Eq.(1). The impact on the predicted t_{SF} values is therefore of exponential character. For example, in the case of ^{252}No , the least action approach leads to the GCM and ATDHFB values $\log_{10} t_{SF} = 3.1819$ (t_{SF} in s) and $\log_{10} t_{SF} = 3.9838$, respectively. They should be compared with the values $\log_{10} t_{SF} = 9.3878$ and $\log_{10} t_{SF}$

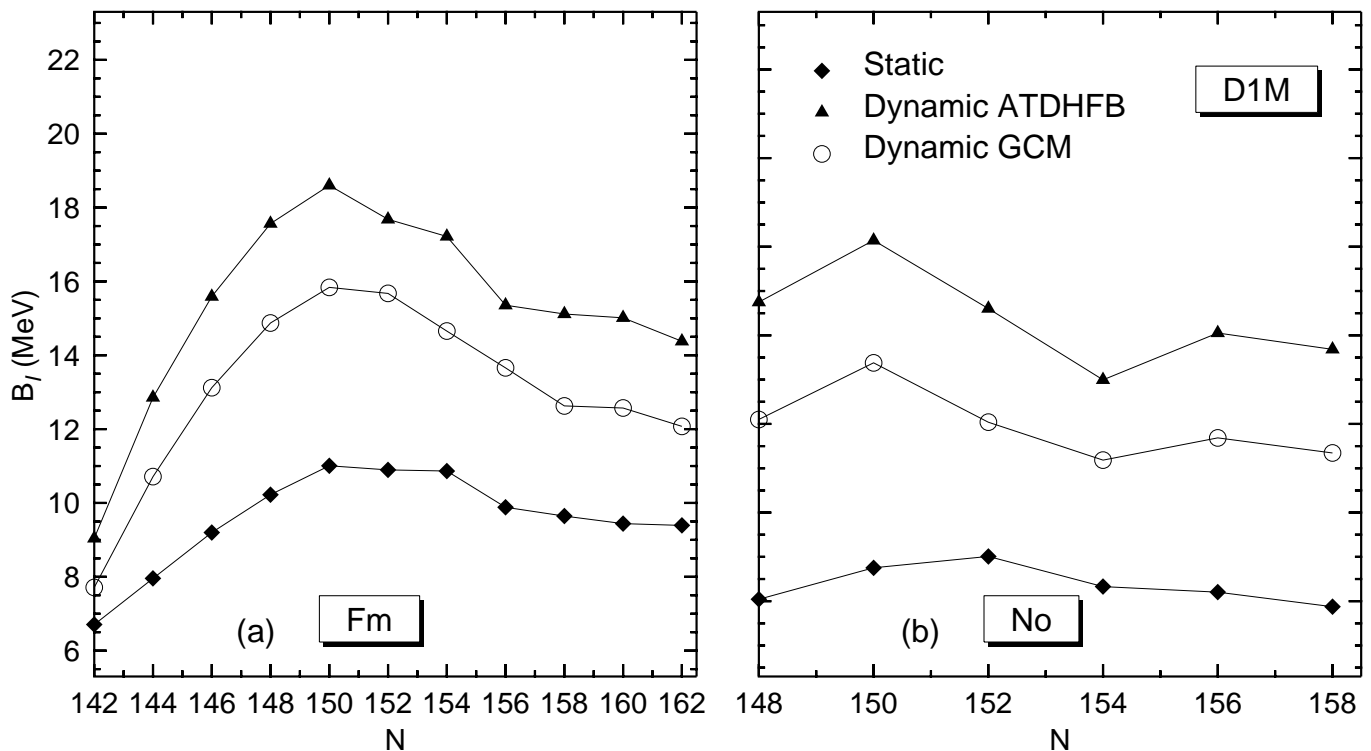


FIG. 6: The inner barrier heights corresponding to the dynamic GCM and ATDHFB fission paths in $^{242-262}\text{Fm}$ and $^{250-260}\text{No}$ are plotted in panels (a) and (b), respectively, as functions of the neutron number. The inner barrier heights corresponding to the static paths in those nuclei are also included in the plot.

$=11.6662$ obtained within the static GCM and ATDHFB schemes [40]. The strong reduction observed in the dynamic GCM and ATDHFB spontaneous fission half-lives, brings them in closer agreement with the experimental value [7].

One important characteristic of the dynamic calculation is its dependence with the parameter E_0 entering the definition of the action Eq. (3). Its role is different from the one of the static case, where E_0 only serves to set up the integration interval in the action. The parameter E_0 can be estimated using the curvature of the energy around the ground state minimum of the fission path and the values of the collective inertias [21, 35]. However, we have followed the usual recipe of considering it as a free parameter. In particular, the results already discussed have been obtained with $E_0 = 0.5$ MeV, a value already employed in previous studies [15, 24, 33–35, 40, 41]. Nevertheless, calculations have also been carried out with $E_0 = 1.0$ MeV [24, 33–35, 40, 41, 54] to test the sensibility of t_{SF} to this parameter. The least action spontaneous fission half-lives for $E_0 = 1.0$ MeV are $\log_{10} t_{SF} = 1.4302$ s (GCM) and $\log_{10} t_{SF} = 2.1485$ s (ATDHFB). Therefore, as in the static approach [24, 33–35, 40, 41], increasing E_0 (from 0.5 to 1.0 MeV) also provides a reduction in the dynamic t_{SF} values. This might lead to a better comparison with the experiment [7]. However, as all the trends with neutron number obtained in this study remain qualitatively the same regardless of the E_0 value used, in what

follows we will restrict our discussions (see, Sec. III B) to those results obtained with $E_0 = 0.5$ MeV.

B. Systematic of the dynamic fission paths and spontaneous fission half-lives in $^{242-262}\text{Fm}$ and $^{250-260}\text{No}$

In Figs. 4 and 5, we have plotted the HFB plus the zero-point rotational energies corresponding to the dynamic ATDHFB and GCM fission paths, as functions of the quadrupole moment Q_{20} , for the nuclei $^{242,246,250,254,258,262}\text{Fm}$ and $^{250,252,256,260}\text{No}$. A similar pattern is exhibited by other Fm and No nuclei and due to this, they are not shown in the figures. Starting from the nuclei ^{246}Fm and ^{252}No , the curves have been shifted by 50 MeV in order to accommodate them in a single plot. The energies corresponding to the static path are also included in the plot. We have followed the same methodology described in Sec. III A for ^{252}No to compute the dynamic paths shown in the figures.

Previous studies within the static framework have pointed out the role of triaxiality for configurations around the top of the inner barrier (see, for example, [10, 26, 33]). Typically, triaxiality reduces the height of the inner barrier by a few MeV. However, the lowering of the inner barrier comes together with an increase of the collective inertia [22, 30] that tends to compensate

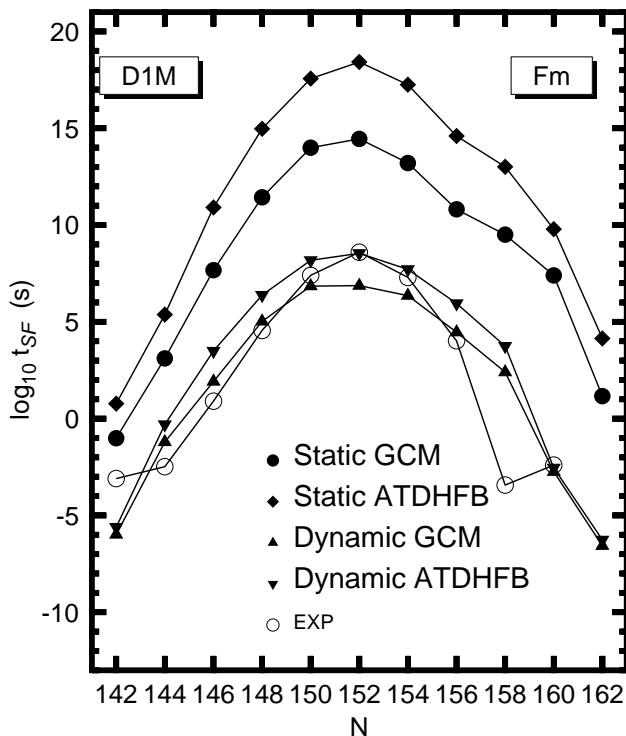


FIG. 7: The spontaneous fission half-lives predicted within the dynamic GCM and ATDHFB schemes for the isotopes $^{242-262}\text{Fm}$ are depicted as functions of the neutron number N . Calculations have been carried out with $E_0 = 0.5$ MeV. Results corresponding to the static GCM and ATDHFB schemes [34] are also included in the plot. The experimental t_{SF} values are taken from Ref. [7].

in the final value of the action. Therefore, the impact of triaxiality in the of t_{SF} value is expected to be very limited and it has not been considered in this study. Previous studies [22] analyzing the dynamic path to fission have corroborated the insignificant role played by triaxiality to determine lifetimes. Moreover, it has also been shown recently, that pairing fluctuations can restore axial symmetry along the fission path [52, 53].

The absolute minima of the static and dynamic paths, shown in Fig. 4, for Fm isotopes correspond to $Q_{20} = 12-16$ b while the top of the inner barriers corresponds to $Q_{20} = 28-36$ b. Fission isomers, located around $Q_{20} = 50-54$ b, are apparent from the paths of $^{242,246,250,254}\text{Fm}$. They are less well defined for isotopes with larger neutron numbers. Similar features are also observed for the static and dynamic paths of the isotopes $^{250,252,256,260}\text{No}$, shown in Fig. 5. The sectors of the fission paths shown in Figs. 4 and 5 where octupole correlations play a key role correspond to quadrupole moments $Q_{20} \geq 60$ b. On the other hand, the most pronounced differences between the static and dynamic paths are found for the excitation energies of the spherical configurations as well as for the inner barrier heights. For example, the inner barrier heights B_I corresponding to the dynamic GCM and ATDHFB fission paths in $^{242-262}\text{Fm}$ and $^{250-260}\text{No}$ are

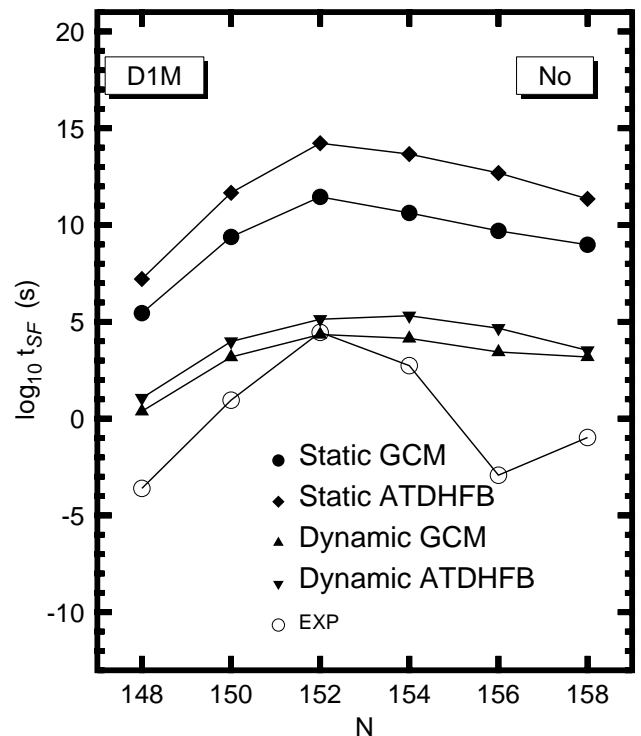


FIG. 8: The spontaneous fission half-lives predicted within the dynamic GCM and ATDHFB schemes for the isotopes $^{250-260}\text{No}$ are depicted as functions of the neutron number N . Calculations have been carried out with $E_0 = 0.5$ MeV. Results corresponding to the static GCM and ATDHFB schemes [40] are also included in the plot. The experimental t_{SF} values are taken from Ref. [7].

plotted in panels (a) and (b) of Fig. 6 as functions of the neutron number N . The inner barrier heights corresponding to the static paths in those nuclei are also included in the plot. In the case of Fm isotopes, the maximum of B_I is reached at $N = 150$ for both the static and dynamic paths. The same is also true for the dynamic paths in No isotopes but, in this case, the maximum static B_I value corresponds to $N = 152$. For both isotopic chains the largest B_I values are the dynamic ATDHFB ones. Let us stress that, as already discussed in Sec. III A, larger dynamic barrier heights arise from the fact that at the Q_{20} -configurations corresponding to the top of the inner barriers the energies display an almost parabolic behavior as functions of the particle number fluctuations $\langle \Delta \hat{N}^2 \rangle$. This combined with a reduction of the collective inertias leads to a minimum of the action for those Q_{20} -constrained configurations.

In Figs. 7 and 8, the spontaneous fission half-lives predicted within the dynamic GCM and ATDHFB schemes are depicted as functions of the neutron number for the nuclei $^{242-262}\text{Fm}$ and $^{250-260}\text{No}$. They are compared with the available experimental data [7]. Results corresponding to the static GCM and ATDHFB schemes are also included in the plot for the sake of comparison. On the one hand, the static approximation already ac-

counts qualitatively for the experimental bell-shaped dependence of the spontaneous fission half-lives as functions of the neutron number [7] in Fm isotopes. However, the least action framework provides, via larger pairing correlations, a reduction of several orders of magnitude in the predicted (dynamic) GCM and/or ATDHFB t_{SF} values. For example, in the case of ^{252}Fm the static GCM and ATDHFB schemes lead to the values $t_{SF} = 2.3950 \times 10^{14}$ s and $t_{SF} = 2.5686 \cdot 10^{18}$ s, respectively [34]. On the other hand the dynamic GCM and ATDHFB values are $t_{SF} = 0.7492 \times 10^7$ s and $t_{SF} = 0.3456 \times 10^9$ s, i.e., the least action approach provides reductions of 7 and 9 orders of magnitude in the predicted spontaneous fission half-lives. As can be seen from Fig. 7, such a reduction of several orders of magnitude occurs for all the considered Fm isotopes and improves dramatically the comparison with the experiment. The same holds true for the No isotopes displayed in Fig. 8, except for the curvature of the experimental values around $N = 152$ that is not yet fully accounted for. Another interesting feature of the results shown in the figures is that the predictions of the static GCM and ATDHFB schemes tend to get closer within the dynamic framework. These results, and the ones obtained in our previous study [44], suggest that the least action framework might be considered a reasonable starting point to improve the predictive power of the HFB approach when applied to the computation of spontaneous fission half-lives.

Other calculations of t_{SF} using the Gogny-D1S [15] or the Skyrme-SkM* EDFs [21] in the static approach lead to a good agreement with the experimental data. This is not the case for our static results with D1M. The reason for the discrepancy with D1S is the smaller collective inertia as compared to the D1M one and consequence of a larger pairing strength in D1S [33]. In the Skyrme-SkM* case, the pairing strength is adjusted to the pairing gaps in ^{252}Fm and therefore, it is very likely that it includes in an effective way other effects beyond the HFB theory that give inertia values better suited to reproduce the experimental t_{SF} .

IV. CONCLUSIONS

In this paper, we have considered a least action approach to compute the spontaneous fission half-lives t_{SF} for a selected set of fermium and nobelium nuclei. To this end, calculations have been carried out within the constrained HFB method and the Gogny-D1M EDF. The

axially symmetric quadrupole moment Q_{20} and the particle number fluctuation $\langle \Delta \hat{N}^2 \rangle$ have been identified as the relevant degrees of freedom for the minimization of the WKB action. The parabolic behavior of the energy as a function of $\langle \Delta \hat{N}^2 \rangle$ together with the corresponding decrease of the (GCM and/or ATDHFB) collective masses leads to a minimum of the action at a $\langle \Delta \hat{N}^2 \rangle$ value larger than the selfconsistent one. As a consequence, the dynamic GCM and/or ATDHFB fission paths exhibit major differences with respect to the static ones for both the spherical configuration as well as for configurations around the top of the inner barriers for all the nuclei studied. As functions of the neutron number, the maxima of the inner barrier heights correspond to $N \approx 152$. Moreover, the larger pairing correlations of the dynamic path with the subsequent reduction of the action, provide dynamic GCM and ATDHFB spontaneous fission half-lives which are several orders of magnitude smaller than the corresponding static predictions improving dramatically the comparison with the available experimental data. It is also found, that the values of t_{SF} predicted within the static GCM and ATDHFB schemes tend to get closer within the dynamic framework. These findings are in line with previous studies in Ref. [44]. The pairing enhancement along the dynamic path could be simulated in an effective way by increasing the pairing strength parameter of the interaction [33].

A long list of task remains to be undertaken. For example, in this work we have resorted to a single constrain on the operator $\Delta \hat{N}^2$ associated with the (total) particle number fluctuations. A more realistic approach could be to consider separate constrains $\Delta \hat{Z}^2$ and $\Delta \hat{N}^2$ on the proton and neutron number fluctuations, respectively. We have considered both the GCM and ATDHFB collective inertias within the perturbative cranking approximation. The use of a nonperturbative approach for the computation of the collective inertias as well as the coupling with degrees of freedom other than the quadrupole one also remain to be explored within the employed least action framework. Work along these lines is in progress and will be reported elsewhere.

Acknowledgments

The work of LMR was partly supported by Spanish MINECO grant Nos FPA2015-65929 and FIS2015-63770.

[1] S. Björnholm and J.E. Lynn, Rev. Mod. Phys. **52**, 725 (1980).
 [2] H.J. Specht, Rev. Mod. Phys. **46**, 773 (1974).
 [3] H.J. Krappe and K. Pomorski, *Theory of Nuclear Fission*, Lectures Notes in Physics, **838** (2012).
 [4] N. Schunck and L. M. Robledo, Rep. Prog. Phys. **79**,

116301 (2016).
 [5] A. Baran, M. Kowal, P. -G. Reinhard, L. M. Robledo, A. Staszczak and M. Warda, Nucl. Phys. A **994**, 442 (2015).
 [6] W. Nazarewicz, Nature Physics, **14**, 537 (2018).
 [7] N. E. Holden and D. C. Hoffman, Pure Appl. Chem. **72**, 1525 (2000).

- [8] P. Ring and P. Schuck, *The Nuclear Many-Body Problem* (Springer, Berlin, 1980).
- [9] J. F. Berger, M. Girod, and D. Gogny, Nucl. Phys. A **428**, 23c (1984).
- [10] J.-P. Delaroche, M. Girod, H. Goutte and J. Libert, Nucl. Phys. A **771**, 103 (2006).
- [11] V. Martin and L.M. Robledo, Int. J. Mod. Phys. E **18**, 788 (2009).
- [12] N. Dubray, H. Goutte and J.-P. Delaroche, Phys. Rev. C **77**, 014310 (2008).
- [13] S. Pérez-Martín and L.M. Robledo, Int. J. Mod. Phys. E **18**, 861 (2009).
- [14] W. Younes and D. Gogny, Phys. Rev. C **80**, 054313 (2009).
- [15] M. Warda, J. L. Egido, L.M. Robledo and K. Pomorski, Phys. Rev. C **66**, 014310 (2002).
- [16] J.L. Egido and L.M. Robledo, Phys. Rev. Lett. **85**, 1198 (2000).
- [17] M. Warda and J.L. Egido, Phys. Rev. C **86**, 014322 (2012).
- [18] N. Nikolov, N. Schunck, W. Nazarewicz, M. Bender and J. Pei, Phys. Rev. C **83**, 034305 (2011).
- [19] J.D. McDonnell, W. Nazarewicz and J.A. Sheikh, Phys. Rev. C **87**, 054327 (2013).
- [20] J. Erler, K. Langanke, H.P. Loens, G. Martínez-Pinedo and P.-G. Reinhard, Phys. Rev. C **85**, 025802 (2012).
- [21] A. Staszczak, A. Baran, W. Nazarewicz, Phys. Rev. C **87**, 024320 (2013)
- [22] A. Baran, K. Pomorski, A. Lukasiak and A. Sobczewski, Nucl. Phys. A **361**, 83 (1981).
- [23] M. Baldo, L.M. Robledo, P. Schuck and X. Viñas, Phys. Rev. C **87**, 064305 (2013).
- [24] S.A. Giuliani and L.M. Robledo, Phys. Rev. C **88**, 054325 (2013).
- [25] Samuel A. Giuliani, Gabriel Martínez-Pinedo, and Luis M. Robledo Phys. Rev. C **97**, 034323 (2018)
- [26] H. Abusara, A.V. Afanasjev and P. Ring, Phys. Rev. C **82**, 044303 (2010).
- [27] H. Abusara, A.V. Afanasjev and P. Ring, Phys. Rev. C **85**, 024314 (2012).
- [28] B.-N. Lu, E.-G. Zhao and S.-G. Zhou, Phys. Rev. C **85**, 011301 (2012).
- [29] S. Karatzikos, A. V. Afanasjev, G. A. Lalazissis and P. Ring, Phys. Lett. B **689**, 72 (2010).
- [30] M. Bender, K. Rutz, P.-G. Reinhard, J.A. Maruhn and W. Greiner, Phys. Rev. C **58**, 2126 (1998).
- [31] T. Bürvenich, M. Bender, J. A. Maruhn, and P.-G. Reinhard, Phys. Rev. C **69**, 014307 (2004)
- [32] K. Rutz, M. Bender, T. Bürvenich, T. Schilling, P.-G. Reinhard, J. A. Maruhn, and W. Greiner Phys. Rev. C **56**, 238 (1997)
- [33] R. Rodríguez-Guzmán and L. M. Robledo, Phys. Rev. C **89**, 054310 (2014).
- [34] R. Rodríguez-Guzmán and L. M. Robledo, Eur. Phys. J. A **50**, 142 (2014).
- [35] R. Rodríguez-Guzmán and L. M. Robledo, Eur. Phys. J. A **52**, 12 (2016).
- [36] S. Goriely, S. Hilaire, M. Girod and S. Péru, Phys. Rev. Lett. **102**, 242501 (2009).
- [37] F. Chappert, M. Girod, and S. Hilaire, Phys. Lett. B **668**, 420 (2008).
- [38] A. Baran, J.A. Sheikh, J. Dobaczewski, W. Nazarewicz and A. Staszczak, Phys. Rev. C **84**, 054321 (2011).
- [39] A. Baran, Phys. Lett. B **76**, 8 (1978).
- [40] R. Rodríguez-Guzmán and L. M. Robledo, Eur. Phys. J. A **52**, 348 (2016).
- [41] R. Rodríguez-Guzmán and L. M. Robledo, Eur. Phys. J. A **53**, 245 (2017).
- [42] S. Pérez-Martín and L.M. Robledo, Phys. Rev. C **78**, 014304 (2008).
- [43] J. Sadhukhan, K. Mazurek, A. Baran, J. Dobaczewski, W. Nazarewicz and J. A. Sheikh, Phys. Rev. C **88**, 064314 (2013).
- [44] S.A. Giuliani, L. M. Robledo and R. Rodríguez-Guzmán, Phys. Rev. C **90**, 054311 (2014).
- [45] L. G. Moretto and R. P. Babinet, Phys. Lett. B **49**, 147 (1974).
- [46] M. Brack, J. Damgaard, A.S. Jensen, H.C. Pauli, V.M. Strutinsky and C.Y. Wong, Rev. Mod. Phys. **44**, 320 (1972).
- [47] G.F. Bertsch and H. Flocard, Phys. Rev. C **43**, 2200 (1991).
- [48] M. Urin and D. Zaretsky, Nucl. Phys. **75**, 101 (1976).
- [49] A. Staszczak, A. Baran, K. Pomorski and K. Böning, Phys. Lett. B **161**.
- [50] K. Pomorski. Int. J. of Mod. Phys. E **16**, 237 (2007).
- [51] A. Staszczak, S. Pilat and K. Pomorski, Nucl. Phys. A **504**, 589 (1989).
- [52] J. Sadhukhan, J. Dobaczewski, W. Nazarewicz, J. A. Sheikh, and A. Baran, Phys. Rev. C **90**, 061304(R) (2014).
- [53] J. Sadhukhan, W. Nazarewicz and N. Schunck, Phys. Rev. C **93**, 011304 (2016).
- [54] J. Zhao, B. -N. Lu, T. Niksic, D. Vretenar and S. -G. Zhou, Phys. Rev. C **93**, 044315 (2016).
- [55] J.F.Berger, M.Girod, D.Gogny, Comp. Phys. Comm. **63**, 365 (1991).
- [56] H. Goutte, J. F. Berger, P. Casoli, and D. Gogny, Phys. Rev. C **71**, 024316 (2005).
- [57] D. Regnier, N. Dubray, N. Schunck, and M. Verriere, Phys. Rev. C **93**, 054611 (2016).
- [58] H. Tao, J. Zhao, Z. P. Li, T. Niksic, and D. Vretenar, Phys. Rev. C **96**, 024319 (2017).
- [59] A. Zdeb, A. Dobrowolski, and M. Warda, Phys. Rev. C **95**, 054608 (2017).
- [60] Y. Tanimura, D. Lacroix, and S. Ayik, Phys. Rev. Lett. **118**, 152501 (2017)
- [61] P. Goddard, P. Stevenson, and A. Rios, Phys. Rev. C **92**, 054610 (2015).
- [62] A. Bulgac, P. Magierski, K. J. Roche, and I. Stetcu, Phys. Rev. Lett. **116**, 122504 (2016)
- [63] C. Simenel, A.S. Umar, arXiv:1807.01859
- [64] R. Rodríguez-Guzmán, L.M. Robledo and P. Sarriguren, Phys. Rev. C **86**, 034336 (2012).
- [65] R. Rodríguez-Guzmán, P. Sarriguren, L.M. Robledo, and J. E. García-Ramos, Phys. Rev. C **81**, 024310 (2010).
- [66] R. Rodríguez-Guzmán, P. Sarriguren, L.M. Robledo, and S. Perez-Martin, Phys. Lett. B **691**, 202 (2010).
- [67] L.M. Robledo, R. Rodríguez-Guzmán, and P. Sarriguren, J. Phys. G: Nucl. Part. Phys. **36**, 115104 (2009).
- [68] L.M. Robledo and R. Rodríguez-Guzmán, J. Phys. G: Nucl. Part. Phys. **39**, 105103 (2012).
- [69] R. Rodríguez-Guzmán, P. Sarriguren, and L.M. Robledo, Phys. Rev. C **82**, 044318 (2010).
- [70] R. Rodríguez-Guzmán, P. Sarriguren, and L.M. Robledo, Phys. Rev. C **83**, 044307 (2011).
- [71] L.M. Robledo and G. F. Bertsch, Phys. Rev. C **84**, 014312 (2011).

- [72] C. Titin-Schnaider and Ph. Quentin, Phys. Lett. B **49**, 213 (1974).
- [73] M. Girod and B. Grammaticos, Nucl. Phys. A **330**, 40 (1979).
- [74] M.J. Giannoni and P. Quentin, Phys. Rev. C **21**, 2060 (1980); Phys. Rev. C **21**, 2076 (1980).
- [75] J. Libert, M. Girod and J.P. Delaroche, Phys. Rev. C **60**, 054301 (1999).
- [76] J.L. Egido and L.M.Robledo, Lectures Notes in Physics **641**, 269 (2004).
- [77] R. Rodríguez-Guzmán, J.L. Egido and L.M. Robledo, Phys. Lett. B **474**, 15 (2000); Phys. Rev. C **62**, 054308 (2000).
- [78] R. Rodríguez-Guzmán, J.L. Egido, and L.M. Robledo, Nucl. Phys. A **709**, 201 (2002).
- [79] G.F. Bertsch, W. Loveland, W. Nazarewicz, and P. Talou, J. Phys. G Nucl. Part. Phys. **42**, 077001 (2015)